JOURNAL OF SPACECRAFT AND ROCKETS
Vol. 31, No. 6, November–December 1994

Aerodynamics of the Shuttle Orbiter at High Altitudes

Didier F. G. Rault*
NASA Langley Research Center, Hampton, Virginia 23681-0001

The high-altitude, high-Knudsen-number aerodynamics of the Shuttle Orbiter are computed from low Earth orbit down to 100 km using three-dimensional direct simulation Monte Carlo and free-molecule codes. Results are compared with the latest Shuttle aerodynamic model, which is based on in-flight accelerometer measurements, and bridging-formula models. Good comparison is observed, except for the normal-force and pitching-moment coefficients. The present results were obtained for a generic Shuttle geometry configuration corresponding to a zero deflection for all control surfaces.

Nomenclature

A, B, C, D	= body-surface elemental-plane coefficients
C_A	= axial-force coefficient
C_D	= drag coefficient
C_L	= lift coefficient
C_m	= pitching-moment coefficient
C_N	= normal-force coefficient
C_p	= pressure coefficient
C_s	= shear coefficient
d_i	= distance to body-surface elemental plane
F_A, F_N	= forces in axial and normal directions, N
L/D	= lift-to-drag ratio
L_{ref}	= reference length, 12.06 m
N/A	= normal-to-axial force ratio
P	= surface pressure, Pa
P_0	= freestream static pressure, Pa
q	= dynamic pressure, $0.5\rho_0 S_{\text{ref}} V_0^2$, Pa
S	= surface shear, Pa
S_{ref}	= reference surface area, 249.909 m^2
V_0	= vehicle velocity, 7500.0 m/s
X, Y, Z	= spatial coordinates
α	= Shuttle incidence angle, deg
ρ_0	= freestream mass density, kg/m^3

Introduction

FLIGHT data recorded during the reentry of the Space Shuttle Orbiter offer the possibility of studying the aerodynamics of an actual flight vehicle over all flow regimes, from the free-molecule regime at orbit altitudes through the transition regime in the 100–200-km range and the continuum hypersonic, supersonic, and subsonic flow regimes at lower altitudes. These data are of special interest in the low-density, high-Knudsen-number domain, in which very few flight data are available to validate simulation codes and methods. The present paper is concerned with the three-dimensional computer simulation of the flowfield around a reentering Shuttle Orbiter from orbit altitude down to 100 km, and the comparison of computed aerodynamic forces and moments with values derived from flight data. Special codes and methods have been developed to perform this simulation. In the high-Knudsen-number flow regime, conventional computational fluid dynamics (CFD) methods, which are based on solving the Navier-Stokes equations, cannot be used.

Instead, we have used a particle simulation approach, namely the direct simulation Monte Carlo method. This method is first described with special emphasis placed on the specific features that make our implementation both relatively easy to set up and computationally efficient. The method is based on Bird's F3 algorithm[1] and has already been used on a variety of problems.[2–5] Two major additions have been made to the method to simulate the Space Shuttle: 1) a solution adaptation and 2) a high-resolution grid definition. This latter feature is necessary to resolve the high-density layer that typically develops on the windside of the relatively cold reentry vehicles. Failure to resolve this region appropriately has been shown to lead to substantial errors in the computation of shear forces and heat transfer rates.[6]

The Shuttle aerodynamic characteristics were computed at five nominal altitudes along the reentry trajectory, namely 100, 110, 120, 145, and 170 km. Results of these calculations and their implications are presented. It is shown that as the Shuttle altitude decreases, the structure of the flowfield gradually changes from a shockless thick compression layer, typical of the free-molecule flow regime, to a viscous-shock layer, and finally to a more continuumlike shock–boundary-layer structure characterized by a strong shock. The computed aerodynamics compare fairly well with flight-data-derived values, except for two instances, namely, the normal-force coefficient and the pitching-moment coefficient. The normal-force coefficient appears to remain close to or above its free-molecule limit value over most of the transition flow regime. This peculiarity is discussed and analyzed. The pitching moment increases significantly with rarefaction, and the center of pressure is found to move forward about 2.5 m from orbit altitude to 100 km. These observations are attributed to a redistribution of the shear and pressure forces on the Shuttle surface. Finally, the aerodynamics of the Shuttle in low Earth orbit (LEO) with open cargo-bay doors are presented.

Simulation Method; Direct Simulation Monte Carlo

In the low-density, high-Knudsen-number flow regime, the computer simulation of flowfields around vehicles can be extremely complex on account of the nonequilibrium at all energy levels. Collisions among gas molecules may be very infrequent, and the gas is typically non-Maxwellian. Simulation methods relying on the Navier-Stokes equations fail because of the breakdown of the Chapman-Enskog relationships for transport properties and the inability to uniquely define a translational temperature. An alternative method, devised by Bird,[7] consists in simulating the gas no longer as a continuous fluid but as a large ensemble of discrete molecules. This method is called the direct simulation Monte Carlo (DSMC), and has been highly documented in the literature and used by several authors in the past 30 years over a wide range of geometries.[1–11]

Recent effort has been aimed at extending the method to allow for the simulation of flowfields around bodies of arbitrarily complex geometry in three dimensions. The code that was used for the present study was originally devised by Bird.[1] It has been further developed by Rault in the course of recent studies on the aerodynamics of slender reentry vehicles (delta wings,[2] waverider[3]), blunt re-entry vehicles (AFE and Viking[4]), satellites,[10] and the self-contamination of satellites.[11] High code efficiency is achieved through the use of a Cartesian unstructured computational grid, as illustrated in Fig. 1,

Received July 19, 1993; revision received March 11, 1994; accepted for publication March 14,1994.

*Aero-Space Technologist, Aerothermodynamics Branch, Space Systems Division. Member AIAA.

Table 1 Gas model

Species	Diam.,[a] Å	Degrees of freedom Rot.	Degrees of freedom Vibr.	Vibr. temp., K	Relaxational collision no. Rot.	Relaxational collision no. Vibr.
O_2	3.96	2	1	2270	5	50
N_2	4.07	2	1	3390	5	50
O	3.00	0	0	—	—	—
N	3.00	0	0	—	—	—
NO	4.00	2	1	2740	5	50

[a] $T_{ref} = 300$ K.

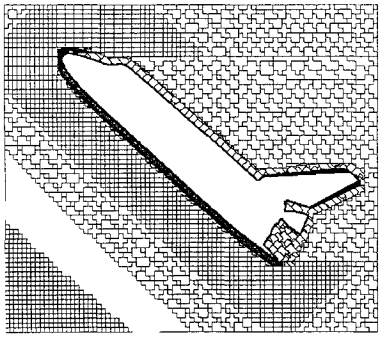

Fig. 1 Computational grid around Shuttle Orbiter at 110 km (before adaptation).

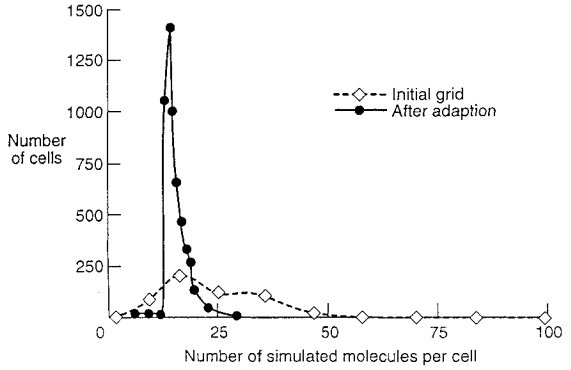

Fig. 2 Distribution of simulated molecules among grid cells after adaptation.

which shows the actual grid used in the simulation of the Shuttle at 110 km and 40-deg angle of attack. The body geometry is defined and stored as an ensemble of cubic elements (pixels), each one being characterized by a wetted surface area and a normal direction cosine. Details on the code setup and performance are described in Ref. 12.

Our present implementation of the DSMC method uses the variable-hard-sphere model to simulate intermolecular collisions,[7] the Larsen-Borgnakke model to evaluate the internal energy transfer among colliding molecules,[7] and Bird's chemistry model.[7] The gas is composed of five species, the characteristics of which have been modeled as shown in Table 1. The molecule-wall interactions are modeled as completely diffuse for both momentum and energy.

Comparison between our three-dimensional DSMC code results and experimental measurements, when available, has shown excellent agreement.[2] The code has been optimized for vector-architecture computers, implemented on parallel processors, and complemented with a set of utilities for diagnosis, preprocessing, and postprocessing.

DSMC Solution Adaptation

Three-dimensional DSMC codes can be highly intensive in CPU time and memory and must be optimally tuned when simulating low-Knudsen-number flowfields. A solution adaptation routine was therefore developed with the following functions.

1) Establish the upstream boundary of the computational domain, by locating the shock-layer leading edge, defined as the surface where the local collision mean free path has increased by 10–20% over the freestream value.

2) Establish the downstream boundary of the computational domain by identifying the flow region that does not affect the vehicle aerodynamics.

3) Restructure the computational grid to ensure that grid cell dimensions are small in comparison with local mean free paths and gradient scales.

4) Adjust the cell volumes so that each cell contains about the same number of simulated molecules. Figure 2 shows the distribution of simulated molecules per cell before and after adaptation. A fairly uniform distribution of the molecules among all cells is important to ensure that the flowfield converges uniformly throughout the computational domain.

5) Adjust the molecular weight factors so that there are about 10–20 molecules per cell on average.

6) Adjust the simulation time step to be smaller than 1) the collision mean time and 2) the molecule residence time in a cell.

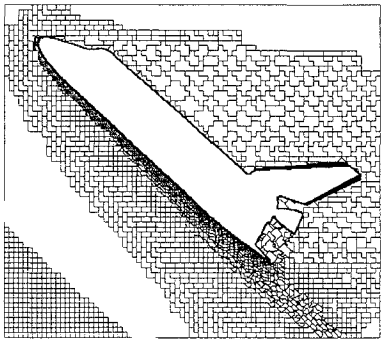

Fig. 3 Computational grid around Shuttle Orbiter at 110 km (after adaptation).

After adaptation, the simulation code is restarted using the previous molecule ensemble, which ensures a fast convergence. Figure 3 shows the computational grid in the Shuttle plane of symmetry after adaptation.

Definition and Resolution of High-Density Windside Body Layer

At hypersonic flight conditions, the ratio of freestream stagnation temperature to body surface temperature is typically high. This high temperature ratio results in large density increases near the body. Within a thin layer along the windside of the vehicle, hereafter referred to as the "body layer," the gas density increases by a factor of 10, reaching values of about 100 times the freestream density on the body surface. In a computer simulation, adequate spatial resolution of the computational grid within this thin layer is crucial for accurately predicting the shear forces on the body surface. As will be shown, these shear forces, which in the continuum flow regime are small with respect to pressure forces, become predominant as the free-molecule flow regime is approached.

Bird's original F3 code is not well suited to simulate either the very thin body layer or the large density increases and would require very large CPU times and memory for typical flight vehicles. A novel method had to be devised to allow one to construct a very high-resolution grid on the windside of the vehicle while retaining the basic F3-code grid structure, which has proven to be

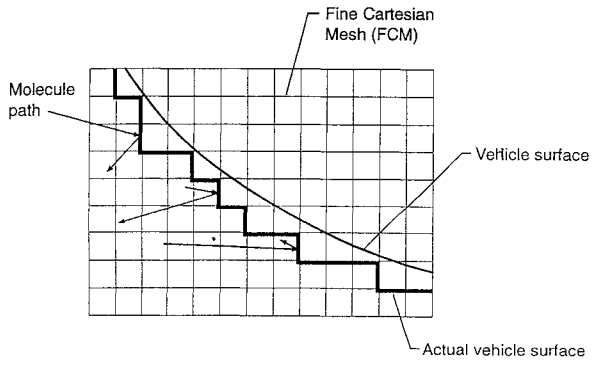

Fig. 4 Surface definition with F3 code.

highly beneficial in terms of ease of code setup and computational efficiency.

The basic F3-code computational grid is constructed on top of two background Cartesian meshes: the coarse Cartesian mesh (CCM), shown in the lower left corner in Fig. 1, and the fine Cartesian mesh (FCM), located near the body surface and in high-density regions. The body surface is discretized at the level of the fine Cartesian mesh, i.e., the body is slightly deformed to conform with the FCM mesh. As shown in Fig. 4, with such a scheme, molecules are reflected on the faces of the cubic pixels and therefore never reach the actual surface of the body. Such an algorithm can safely be used when simulating flowfields at high Knudsen numbers or for wind-tunnel conditions (where the ratio of stagnation temperature to body surface temperature is typically low), but not for flight conditions, at which the body layer may be much thinner than the optimal pixel dimensions. In the case of the Space Shuttle at altitudes lower than 120 km, optimal pixel size is about 10–20 cm, depending on the CPU memory available, whereas the windside body-layer thickness is on the order of a few centimeters.

The approach that was devised to define the body layer on the windside of reentry vehicles is schematically illustrated in Fig. 5a. The body surface is decomposed into a series of planes, one for each body pixel. Each plane is characterized by an equation of the type

$$Ax + By + Cz + D = 0$$

where A, B, C are the normal direction cosines and D is the distance of the plane to the reference-frame origin. The computational grid in the body layer is constructed with a series of planes parallel to the body planar surface elements. The equations of each of these planes is typically

$$Ax + By + Cz + D - d_i = 0$$

where A, B, C, D are the plane coefficients corresponding to the closest body pixel and d_i is the distance of the plane to the body plane. As illustrated in Fig. 5a, the body layer is broken down into a series of layers at distances $d_1, d_2, \ldots, d_N$ from the body planes. These distances are read from an input file and could readily be changed during the course of a simulation to adjust the grid thickness according to the value of the local mean free path. To sample surface properties, several adjacent body pixels are grouped together into "surface sampling zones," as shown in Fig. 5b. The body and flow pixels associated with the body pixels belonging to a given surface sampling zone form a stack of cells, as illustrated in Fig. 5b, each cell being numbered as follows.

1) Cells 1 to M_{zone} for the first layer, where M_{zone} is the total number of surface sampling zones adjacent to the body layer.

2) Cells $(N-1)M_{\text{zone}}+1$ to NM_{zone} for the Nth layer.

Molecules entering the body layer are assigned to their cells through a series of cross-reference arrays. A molecule at a point (X, Y, Z) is known to be within pixel (NX = X/DP, NY = Y/DP, NZ = Z/DP), where DP is the cubic pixel dimension. Through a preset table, the pixel (NX, NY, NZ) is associated with the body surface pixel k, which is characterized by normal direction cosines

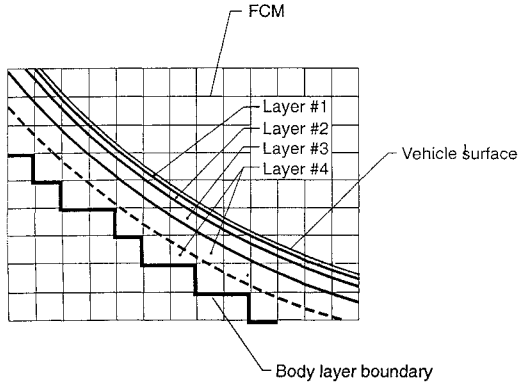

Fig. 5a High-resolution grid within windside body layer: cell layers.

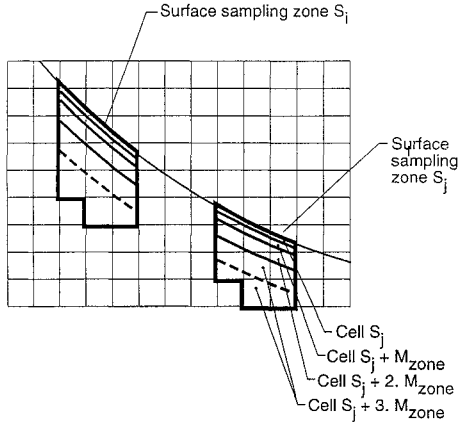

Fig. 5b High-resolution grid within windside body layer: computational cells.

(A_k, B_k, C_k) and a constant D_k. The distance from the molecule to the body plane is therefore

$$\text{dist} = A_k X + B_k Y + C_k Z + D_k$$

The layer L containing the molecule is defined as the layer that satisfies the condition

$$d_{L-1} < \text{dist} < d_L$$

Finally, the cell N containing the molecule is

$$N = J_{\text{zone}} + (L-1)M_{\text{zone}}$$

where J_{zone} is the surface sampling zone containing body pixel k.

This algorithm has several merits. It allows the user to set up the near-body grid to any arbitrary high resolution. Moreover, since molecules are assigned to their cells through a distance computation and cross-reference arrays, the tracking of molecules within the body layer is computationally fast. This algorithm has been implemented for arbitrary geometry, and the details specific to the Space Shuttle application are described in Ref. 12.

Flow Conditions, Atmospheric Properties, and Vehicle Geometry

As the Shuttle orbiter reenters the atmosphere from orbit down to 100 km, it traverses a flight domain where the Knudsen and Reynolds numbers vary by several orders of magnitude, as illustrated in Fig. 6, which shows the re-entry trajectory of the Shuttle in a Mach–Reynolds–Knudsen-number domain. The Reynolds and Knudsen numbers are based on the vehicle length and the vehicle orbital velocity of 7500 m/s. For Knudsen numbers larger than 10, the flow regime is free-molecular, i.e., the aerodynamics of the vehicle depend little on collisions among gas molecules, and for a convex body shape such as the Shuttle Orbiter, the forces and moments can be evaluated semianalytically.[7] In the transition domain, which extends down from Knudsen numbers of 10 at least to

0.01 (Shuttle altitudes of 200 km down to 100 km, approximately), a particle-tracing code, such as the DSMC code described above, must be used. The DSMC code, however, becomes extremely difficult to use and requires large amount of computer time and memory when Knudsen numbers are less than 0.01.

Table 2 shows the atmospheric conditions that were assumed at the five nominal altitudes considered in this study. The atmospheric densities can be seen to vary nearly 3 orders of magnitude over the 100- to 170-km altitude range.

The Shuttle Orbiter geometry was obtained from NASA Johnson Spaceflight Center as a file of discrete data points, each being defined by three spatial coordinates. The original geometry corresponded to a body-flap deflection of 0 deg, an inboard elevon deflection of 10 deg, an outboard elevon deflection of 5 deg, and closed cargo-bay doors. Using data on the hinge line of the control surfaces and cargo-bay doors, it was possible to generate data files corresponding to arbitrary control-surface deflections and cargo-bay door configuration. The results presented herein were obtained with 0-deg deflection for all control surfaces. The cargo-bay doors are closed in the re-entry phase and open in orbit.

Simulated Flowfield around the Shuttle Orbiter

The structure of the flowfield around a re-entering Shuttle Orbiter is illustrated in Figs. 7 and 8, which show the total gas density around the vehicle as altitudes decrease from 170 to 100 km. Densities are shown normalized to the undisturbed freestream density. At 170 km, the flow disturbance extends far away from the Shuttle surface and the computational domain is consequently large. Collisions among gas molecules are rare, and the Shuttle "snowplows" into the ambient atmosphere. The molecules that reach the vehicle surface lose most of their energy and momentum as they diffusely reflect on the surface, and then slowly travel to the boundary of the computational domain, with little chance of colliding with incoming molecules. No shock is formed, since gas molecules interact little with each other. As the altitude is decreased, the extent of the flow disturbance upstream of the Shuttle decreases, which allows for a reduction of the size of the computational domain. Collisions among gas molecules are more frequent, and density gradients steepen. At 100 km, a shock front can clearly be seen to have formed. It is characterized by a rapid density increase from 1 to 4 times the freestream density. The density also increases very sharply near the vehicle surface. Figures 9 and 10 show the density profile along the stagnation streamline at 120 and 100 km, respectively. At 100 km, the density

Table 2 Nominal atmospheric properties

Nominal alt., km	No. density, molecules/m^3	Temp., K	Molar composition		
			O_2	N_2	O
100	1.20×10^{19}	193.7	0.18	0.78	0.04
110	2.20×10^{18}	250.0	0.12	0.77	0.11
120	5.77×10^{17}	335.0	0.08	0.74	0.18
145	6.56×10^{16}	628.0	0.055	0.622	0.323
170	2.06×10^{16}	790.4	0.040	0.523	0.437

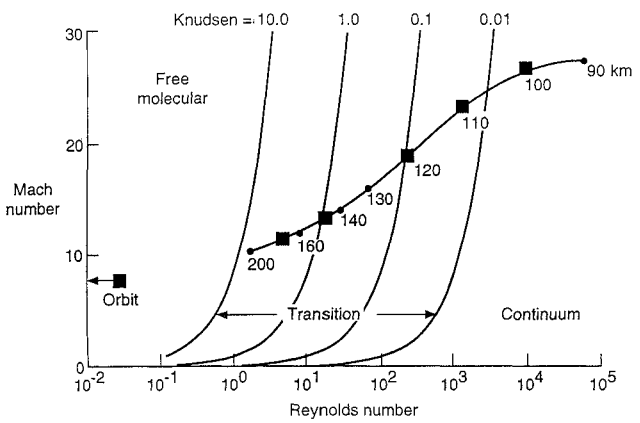

Fig. 6 Shuttle trajectory in Reynolds–Mach–Knudsen-number domain.

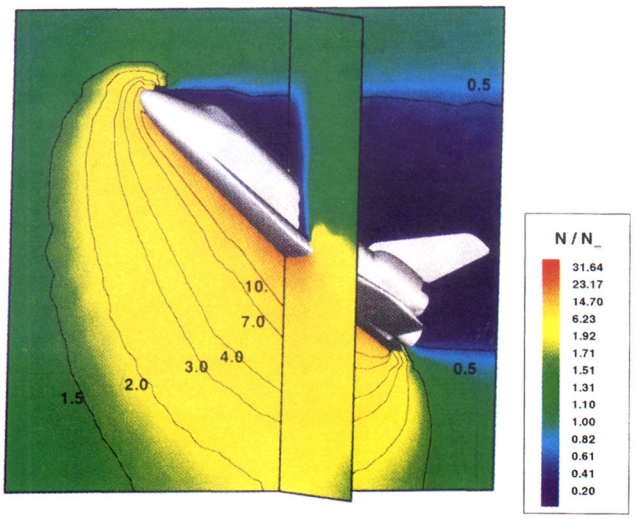

Fig. 7 Total-density map around Shuttle Orbiter at 170-km altitude.

can be seen to increase 5-fold within 1 cm of the surface, reaching a value of 220 times the freestream value near the vehicle surface. It must be noted here, however, that this latter value is an overestimate of actual gas density near the vehicle surface. All the computations presented herein assume that the Shuttle surface is still cold and isothermal at 300 K, whereas thermocouple measurements on the windward surface indicate[13] that at 100 km the temperature near the stagnation point may be in the range of 600 to 800 K. Figures 9 and 10, however, do show the capability of our present code for adequate spatial resolution of the thin subcentimeter body layer (to within a local mean free path) over the 32-m-long Shuttle Orbiter. Additional computations performed with isothermal surface temperature of 600 K show very little effect on the overall aerodynamic properties of the vehicle.

Aerodynamic Characteristics: Comparison with Flight Data

Normal-to-Axial Force Ratio

Blanchard[14–16] has used high-sensitivity micro-g accelerometers to measure forces on the Shuttle Orbiter during re-entry in the altitude range of 60 to 160 km. The aerodynamic forces F_A and F_N in the axial and normal directions are derived from the measured data upon removal of the effects of thrust, rotational acceleration, auxiliary power unit (APU) exhaust plumes, and control-surface deflection. The force ratio F_N/F_A is of special interest in that it is independent of the dynamic pressure, i.e., atmospheric density and Orbiter reentry velocity. Figure 11 compares Blanchard's reduced data with the results of our DSMC computation. Table 3 summarizes the DSMC results. All the results refer to zero deflection for the elevons and body flap. Good agreement can be observed over the whole altitude range considered in this study. Also shown in Fig. 11 are the results obtained with the DSMC code run in a collisionless mode. In this mode, free-molecular conditions are simulated, which, by comparison, allows one to quantify the transitional effects, i.e., the effects of intermolecular collisions on the aerodynamics. It can be observed that these effects seem to disappear at 170 km, where the DSMC transitional and free-molecular results converge. Preflight estimates for the normal-to-axial force ratio are also shown in Fig. 11.[17] These early estimates appear to be somewhat low. Finally, results obtained using Potter's bridging formula[18] are shown. This bridging formula is based on wind-tunnel and early Shuttle data, and good agreement can be observed with Blanchard's model.

Lift-to-Drag Ratio

The lift-to-drag ratio L/D can be derived from F_N/F_A if the incidence angle α is known:

$$\frac{L}{D} = \frac{F_N/F_A - \tan\alpha}{1 + F_N/F_A} \tag{1}$$

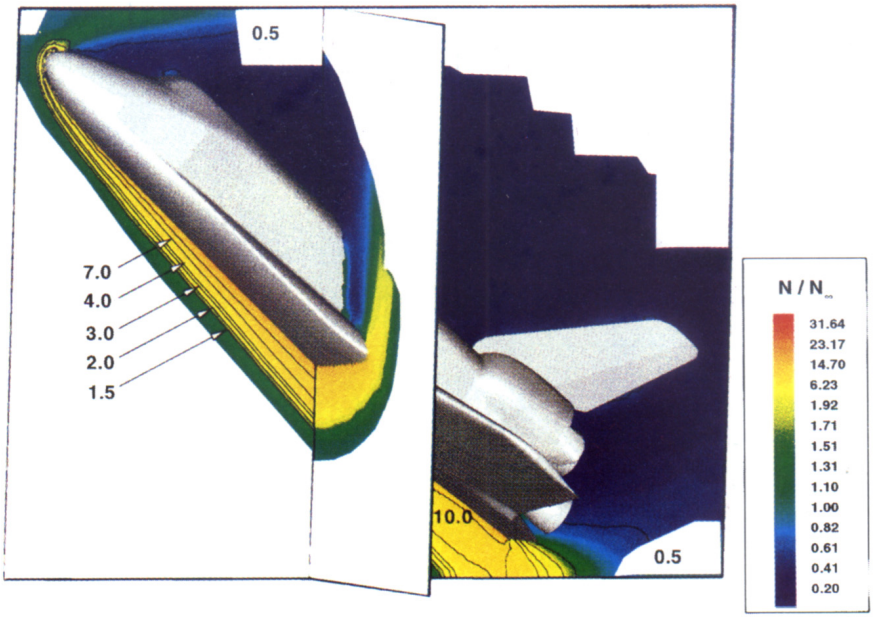

Fig. 8 Total-density map around Shuttle Orbiter at 100-km altitude.

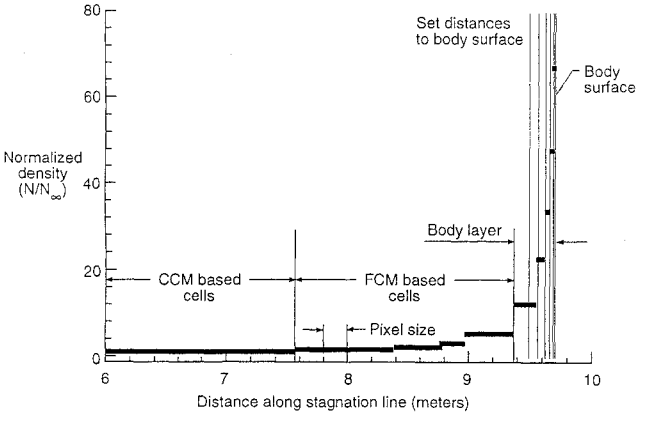

Fig. 9 Density profile along stagnation streamline on Shuttle Orbiter at 120-km altitude.

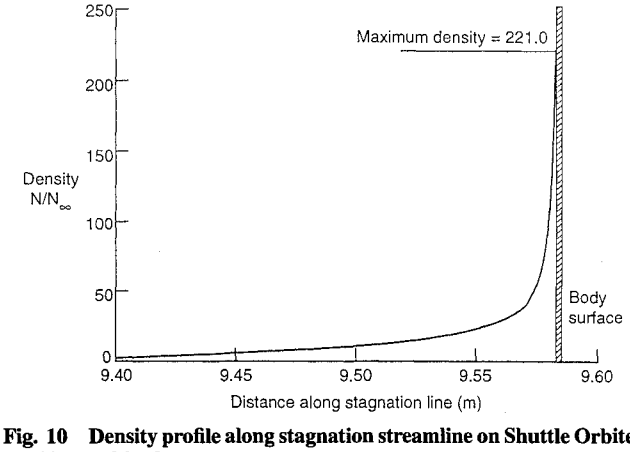

Fig. 10 Density profile along stagnation streamline on Shuttle Orbiter at 100-km altitude.

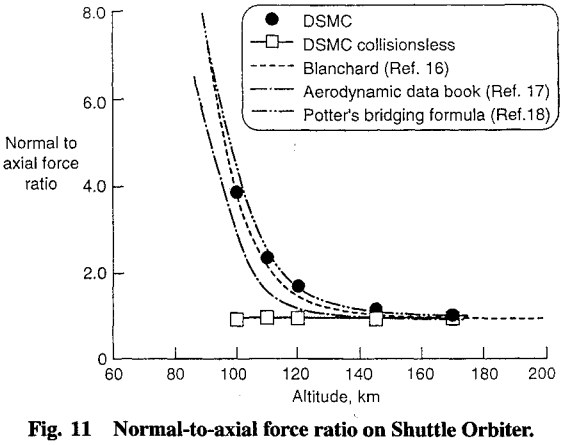

Fig. 11 Normal-to-axial force ratio on Shuttle Orbiter.

This ratio is also independent of the dynamic pressure. Figure 12 shows L/D computed with the DSMC code run in the transitional and collisionless modes. The results are compared with wind-tunnel data (corresponding to altitudes lower than 90 km) and flight data. The gray band shown in the figure corresponds to a series of Shuttle flights, each one occurring at different elevon and body-flap deflection angles and different atmospheric conditions.[15] The gray-band data were not corrected for control-surface deflection angle, i.e., these data were not reduced to a zero deflection angle. Agreement between computed results and flight data can be observed to be quite good over the whole range of altitudes considered in the present work. The results obtained by Bird[1] using an early version of the F3 code are also shown for comparison. The modified Newtonian limit, corresponding to a hypersonic inviscid flow, is shown to be $L/D = 1.10$, which is very close to the value $L/D = 1.06$ computed by Weilmuenster et al.[19] using the continuum-fluid LAURA code. Figure 13 shows that the preflight estimates for L/D ratio are somewhat smaller than the measured values. Also shown are Blanchard's proposed aerodynamic model, which is based on flight data,[16] and Potter's bridging formula.

Axial Coefficient

The unambiguous determination of the axial and normal coefficients C_A and C_N from the axial and normal accelerometer measurements would require the simultaneous measurement of the freestream dynamic pressure or, alternatively, the atmospheric density and vehicle velocity. However, in situ measurements of atmospheric density cannot readily be done between 90 km and low-Earth orbit altitude. To estimate C_A and C_N from flight data, Blanchard had to devise an iterative procedure as described in Ref. 14. Figure 14 compares the DSMC-computed values of the axial coefficient with the values obtained by Blanchard and using Potter's bridging formula. Good agreement can be observed at all altitudes, which might be surprising in view of the fact that the actual atmospheric conditions prevailing during flight are known to be different from the standard conditions used in our DSMC computations. The preflight

Table 3 DSMC numerical results: aerodynamic coefficients

Altitude, km	Drag C_D	Life C_L	Axial C_A	Normal C_N	Pitching moment C_m around c.g.	Center of pressure w.r.t. C.G., m	L/D
100	1.15	0.824	0.354	1.37	−0.0980	−0.861	0.714
110	1.38	0.696	0.606	1.42	−0.145	−1.24	0.506
120	1.65	0.564	0.901	1.49	−0.207	−1.68	0.342
145	1.97	0.297	1.32	1.49	−0.286	−2.31	0.151
170	2.07	0.193	1.46	1.48	−0.293	−2.39	0.0931

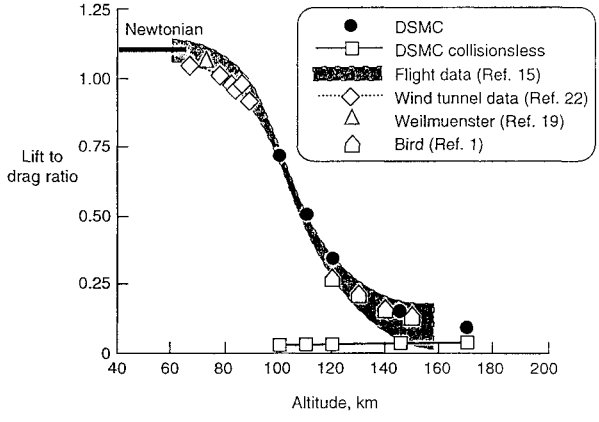

Fig. 12 Lift-to-drag ratio on Shuttle Orbiter.

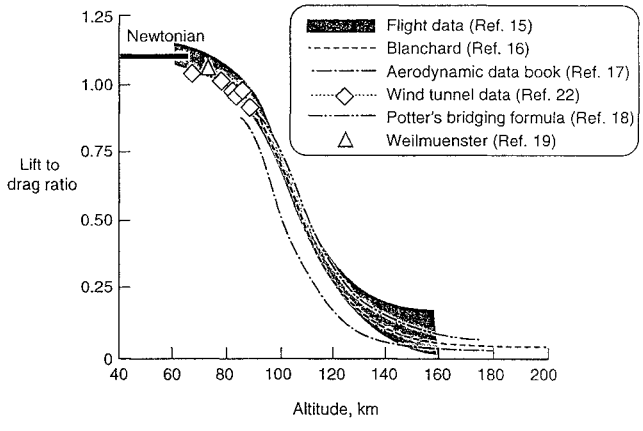

Fig. 13 Lift-to-drag ratio on Shuttle Orbiter.

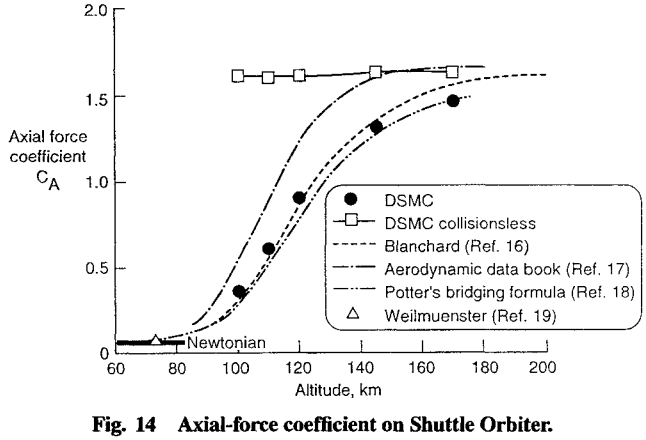

Fig. 14 Axial-force coefficient on Shuttle Orbiter.

estimates, however, can be seen to overestimate C_A significantly. When comparing the transition and collisionless DSMC results, it can be observed that, for the axial force, transition-flow effects are still significant at 170 km.

Normal Coefficient

Figure 15 compares the computed values of the normal coefficient with Blanchard's proposed model and Potter's bridging formula. A

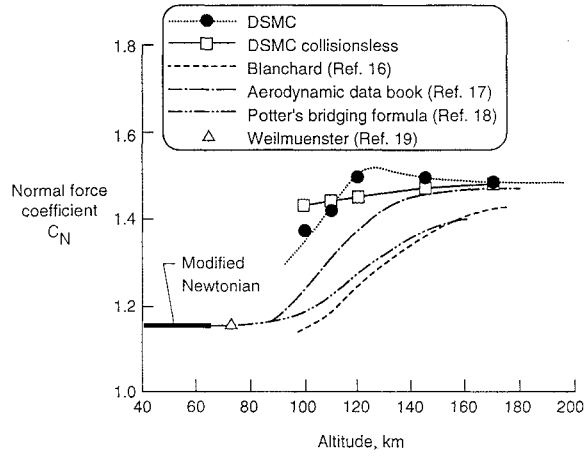

Fig. 15 Normal-force coefficient on Shuttle Orbiter.

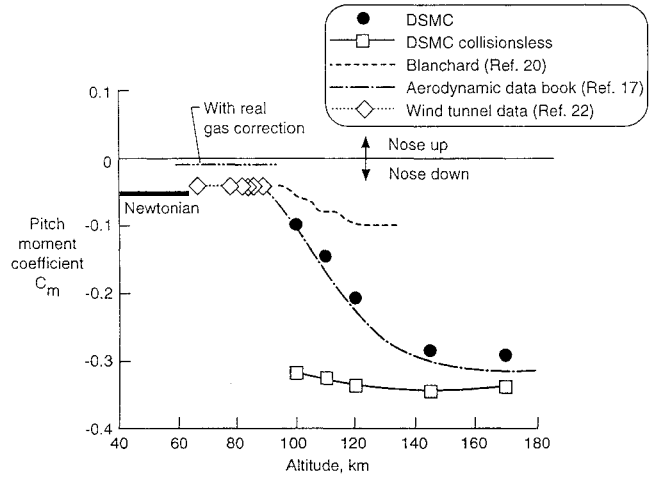

Fig. 16 Pitching-moment coefficient on Shuttle Orbiter.

fairly large discrepancy, up to 20%, can be observed between the DSMC computation and Blanchard's model. Moreover, when comparing the transitional and collisionless DSMC results, it can be seen that C_N does not increase monotonically from the low continuum-flow values to the higher free-molecular values. Instead, C_N reaches a maximum within the transitional domain at about 120 km, and then decreases afterwards towards the free-molecular limit. This singular behavior of the normal coefficient is discussed in the next section. Neither Blanchard's proposed model nor Potter's bridging formula reproduces this behavior. The preflight estimates of C_N appear to be closer to our present results, but do not predict the "overshoot" observed with DSMC.

Pitching Moment

Figure 16 shows the pitching moment around the Shuttle Orbiter nominal center of gravity located at Shuttle coordinates $x = 1076.7$ in., $z = 375.0$ in. Rarefaction effects can be seen to increase the magnitude of the pitching moment from the modified Newtonian value, which is close to wind-tunnel measured data, to the free-molecular limit value. This pitching-moment increase is due to a redistribution of the pressure and shear forces acting on the Shuttle surface, as will be shown below. Our present results are compared with the

ones obtained by Blanchard and Hinson.[20] They used the rate of change of the Orbiter effective incidence angle between two control thruster firings to evaluate the overall pitching moment acting on the Shuttle body. The contribution of aerodynamics to the overall pitching moment was deduced upon removal of the effects of APU exhaust and gravity gradients. Blanchard's reduced data, shown in Fig. 16, correspond to a zero deflection angle for the elevons and body flap. Figure 16 shows that our present results differ markedly from the ones derived by Blanchard. This might in part be due to the fact that, at the highest altitudes, the aerodynamic contribution to the pitching moment is very small compared with the effects of the APU exhaust, and large errors may therefore be introduced in the flight-data reduction procedure.

The rarefaction effects on forces and moments result in a shift of the center of pressure in the forward direction by about 2.5 m as the Shuttle descends from LEO to 100 km.

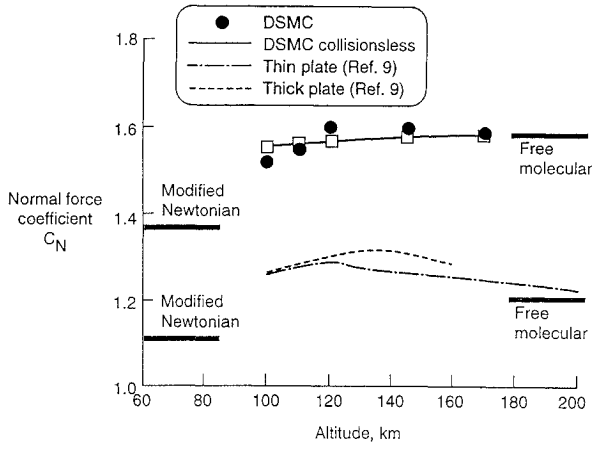

Fig. 17 Normal-force coefficient on Shuttle Orbiter and flat plates.

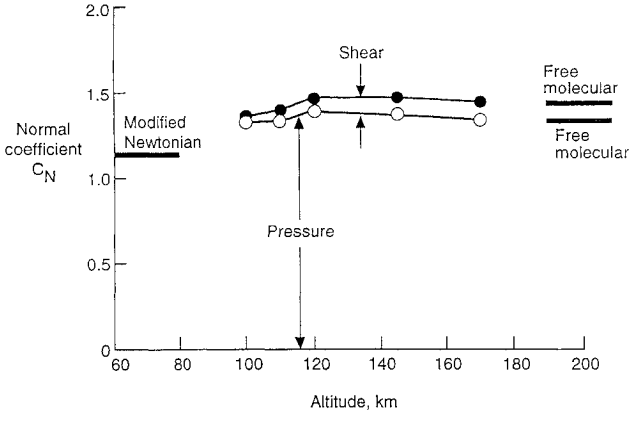

Fig. 18 Pressure and shear contribution to normal-force coefficient.

Analysis of the Normal-Force Coefficient

The singularity in C_N observed in our present DSMC computation, namely, the overshoot over both continuum and free-molecular values, had been observed earlier by Dogra and Moss[9] in their study of flat plates at 40-deg incidence. Their results, which are reproduced in Fig. 17, were obtained with the two-dimensional DSMC code devised by Bird.[7] A thorough analysis of this overshoot needs to be conducted, but a few remarks can already be made at this point. Figure 18 shows that the aerodynamic force on the Shuttle in the normal direction is mostly due to pressure forces. The shear, or friction, forces contribute little to C_N and mainly affect the axial forces. For a flat plate, C_N is entirely due to pressure forces. The overshoot in C_N is therefore due to an overshoot of the pressure forces on the vehicle, that is, an overshoot of the normal momentum transfer from the gas molecules to the surface. Koppenwallner and Legge[21] have identified and explained a similar overshoot on the drag coefficient of simple geometries. They have argued that, at high Mach numbers, freestream molecules that in the free-molecular regime would not reach the body surface are scattered within the high-density gas cloud developing on the windside and redirected towards the vehicle surface. Figure 19 schematically illustrates this flux- and pressure-enhancing effect.

Surface Forces

The magnitude and distribution of the pressure and shear forces on the Shuttle windside surface vary with altitudes as illustrated in Figs. 20 and 21. These figures show the pressure and shear coefficients C_p and C_s, which are defined as follows:

$$C_p = (P - P_0)/q \qquad C_s = S/q \tag{2}$$

where P, S, q are, respectively, the pressure (i.e., normal momentum flux) and shear (i.e., tangential momentum flux) and the dynamic pressure. The quantity P_0 is the freestream pressure. At high altitudes (above 120 km), the pressure forces appear to be fairly uniform over the whole windside of the Shuttle, with maxima near the stagnation point and the wing leading edge. At the lower altitudes, the pressure is mostly acting on the stagnation region and the wing leading edge.

The shear forces uniformly decrease in magnitude from 170 to 100 km, as shown in Figs. 22 and 23. Moreover, they appear to be fairly uniform over the windside at the higher altitudes, with a minimum in the stagnation region. At the lower altitudes, high shear forces can be seen to develop near the wing leading edge.

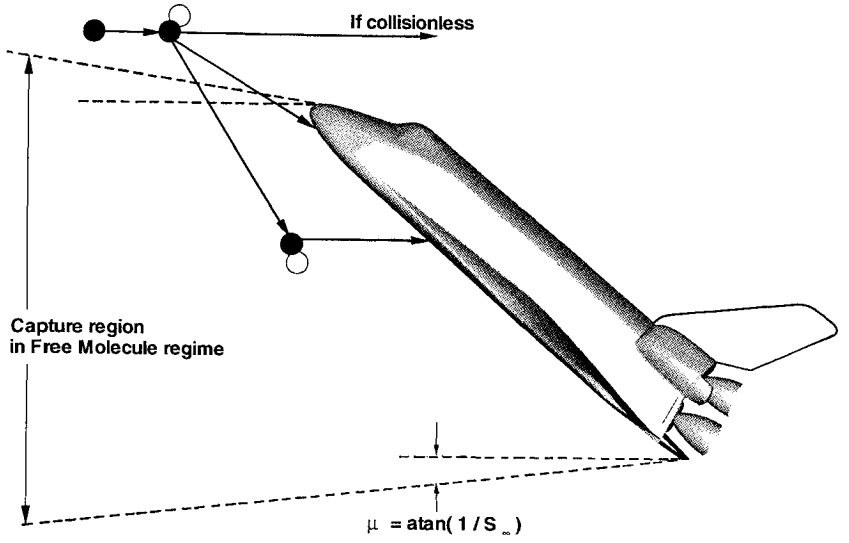

Fig. 19 Mechanism enhancing particle flux and momentum transfer.

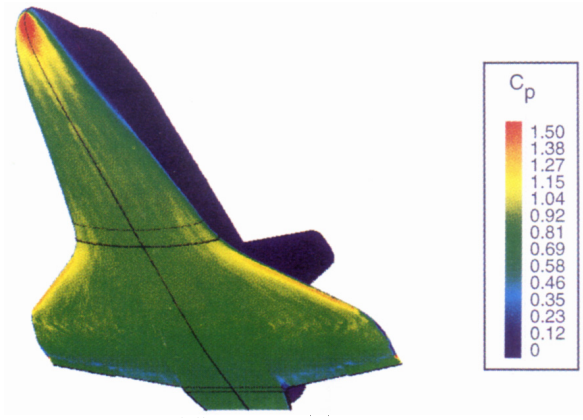

Fig. 20 Pressure force distribution on Shuttle Orbiter at 170 km.

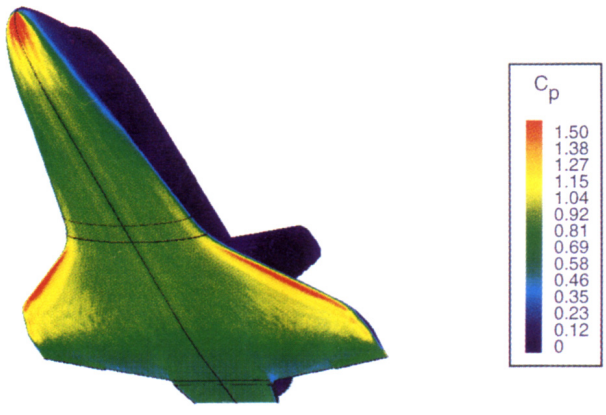

Fig. 21 Pressure force distribution on Shuttle Orbiter at 110 km.

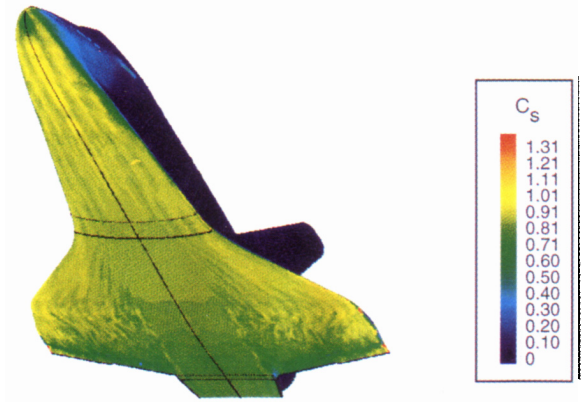

Fig. 22 Shear force distribution on Shuttle Orbiter at 170 km.

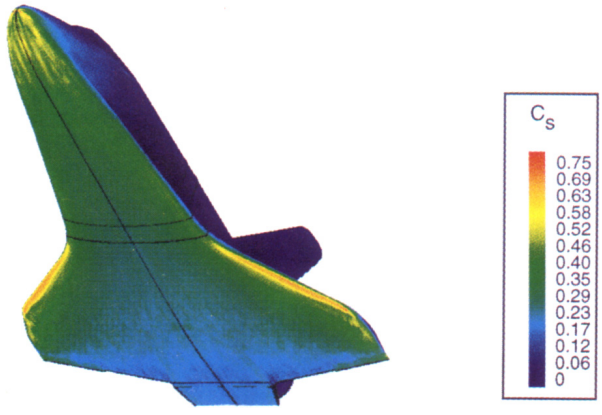

Fig. 23 Shear force distribution on Shuttle Orbiter at 110 km.

Table 4 Comparison of collisionless DSMC and free-molecular (FM) results

Altitude, km	Code	Drag, C_D	Life, C_L	Axial, C_A	Normal, C_N
100	DSMC	2.15	0.0621	1.61	1.43
	FM	2.12	0.0735	1.58	1.42
110	DSMC	2.15	0.0708	1.60	1.44
	FM	2.13	0.0759	1.58	1.43
120	DSMC	2.16	0.0746	1.61	1.45
	FM	2.14	0.0785	1.59	1.44
145	DSMC	2.19	0.0787	1.63	1.47
	FM	2.22	0.0870	1.64	1.49
170	DSMC	2.19	0.0845	1.63	1.48
	FM	2.22	0.0923	1.64	1.50

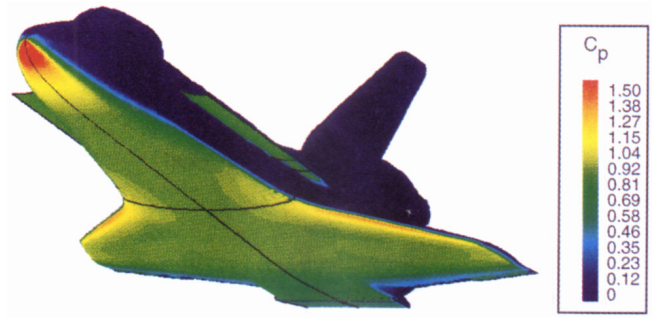

Fig. 24 Pressure force distribution on Shuttle Orbiter in orbit at 40-deg incidence.

Fig. 25 Shear force distribution on Shuttle Orbiter in orbit at 40-deg incidence.

Orbit Aerodynamics: Free-Molecular Simulation

In orbit, the atmosphere density is very low, and intermolecular collisions have little effects on the aerodynamics of the vehicle. The aerodynamic forces and moments on an orbital vehicle can be computed independently with either a DSMC code run in a collisionless mode or semianalytical free-molecule code. The free-molecule code developed by Rault[10] was used to evaluate the aerodynamic characteristics of an orbiting Shuttle at 40-deg incidence with an open cargo-bay door. Results are shown in Figs. 24 and 25 in the form of pressure and shear coefficients on the vehicle surface. These results can be observed to be very similar to the ones obtained with the DSMC code at 170 km. Table 4 provides a further comparison between the collisionless DSMC and free-molecule codes. This table shows the aerodynamic force and moment coefficients computed for a closed cargo-bay configuration using the collisionless DSMC and the free-molecule codes for altitudes ranging from 100 to 170 km. Good agreement can be observed between the particle-tracing DSMC code and the semianalytical free-molecule code.

Conclusion

A simulation of the flowfield around the Shuttle Orbiter during the early phase of its re-entry into the Earth atmosphere has been conducted. Computations have been performed for altitudes ranging from LEO down to 100 km. The present work was primarily

done using a three-dimensional direct simulation Monte Carlo code, which allowed us to simulate and analyze the highly nonequilibrium flowfield over a wide range of Knudsen numbers. For this task, the code was specially enhanced to allow for the spatial resolution of high density gradients, which typically develop near the windside surface of re-entry vehicles. The aerodynamic force and moment coefficients were evaluated. Fairly good agreement has been found with Blanchard's proposed aerodynamic model, which is based on highly sensitive accelerometer data measured in flight. Major discrepancies, however, have been observed regarding the normal coefficient C_N and the pitching moment. Our computations show that C_N is characterized by an overshoot in the transition domain, similar to the one observed in an earlier two-dimensional DSMC simulation over flat plates at incidence. If confirmed, such an overshoot should be taken into account in future reduction of flight data. Our values for the pitching moment seem to indicate that the center of pressure is further aft than predicted by Blanchard.

References

[1]Bird, G. A., "Application of the Direct Simulation Monte Carlo Method to the Full Shuttle Geometry," AIAA Paper 90-1962, June 1990.

[2]Rault, D. F. G., Wilmoth, R. G., and Bird, G. A., "An Efficient DSMC Algorithm Applied to a Delta Wing," AIAA Paper 91-1316, June 1991.

[3]Rault, D. F. G., "Aerodynamic Characteristics of a Hypersonic Viscous Optimized Waverider at High Altitudes," AIAA Paper 92-0306, Jan. 1992.

[4]Rault, D. F. G., "Towards an Efficient Three Dimensional DSMC Code for Complex Geometry Problems," *Rarefied Gas Dynamics: Theory and Simulations*, edited by B. D. Shizgal and D. P. Weaver, Vol. 159, Progress in Astronautics and Aeronautics, AIAA, Washington, DC, in press.

[5]Moss, J. N., Rault, D. F. G., and Price, J. M., "DSMC Simulations of Hypersonic Viscous Interactions Including Separation," *Rarefied Gas Dynamics: Space Science and Engineering*, edited by B. D. Shizgal and D. P. Weaver, Vol. 160, Progress in Astronautics and Aeronautics, AIAA, Washington, DC, in press.

[6]Moss, J. N., and Bird, G. A., "Direct Simulation of Transitional Flow for Hypersonic Re-Entry Conditions," *Progress of Astronautics and Aeronautics*, edited by H. F. Nelson, Vol. 96, 1984, pp. 113–139.

[7]Bird, G. A., *Molecular Gas Dynamics*, Clarendon Press, Oxford, 1976.

[8]Bird, G. A., "Monte Carlo Simulation in an Engineering Context," *Rarefied Gas Dynamics*, edited by Sam S. Fisher, Vol. 74, Progress in Astronautics and Aeronautics, AIAA, Washington, DC, 1981, pp. 235–239.

[9]Dogra, V. K., and Moss, J. N., "Hypersonic Rarefied Flow About Plates at Incidence," AIAA Paper 89-1712, Jan. 1989.

[10]Rault, D. F. G., "Aerodynamic Characteristics of Magellan Spacecraft in Venus Upper Atmosphere," AIAA Paper 93-0723, Jan. 1993.

[11]Rault, D. F. G., and Woronowicz, M. S., "Spacecraft Contamination Investigation by Direct Simulation Monte Carlo. Contamination on UARS/HALOE," AIAA Paper 93-0724, Jan. 1993.

[12]Rault, D. F. G., "Aerodynamics of Shuttle Orbiter at High Altitudes," AIAA Paper 93-2815, July 1993.

[13]Hartung, L. C., and Throckmorton, D. A., *Space Shuttle Entry Heating Data Book*, Vol. I-STS 2, NASA Pub. 1191, April 1992.

[14]Blanchard, R. C., Larman, K. T., and Barrett, M., "The High Resolution Accelerometer Package (HiRAP) Flight Experiment Summary for the First 10 Flights," NASA Pub. 1267, April 1992.

[15]Blanchard, R. C., "Rarefied Flow Lift-to-Drag Measurements of the Shuttle Orbiter," 15th Congress of International Council of Aeronautical Sciences (ICAS), Paper ICAS-86-2.10.2, Sept. 1986.

[16]Blanchard, R. C., Larman, K. T., and Moats, C. D., "Rarefied-Flow Shuttle Aerodynamics Flight Model," NASA TM-107698, Feb. 1993.

[17]*Aerodynamic Design Data Book. Volume I. Orbiter Vehicle*, NASA CR-160386, 1978.

[18]Potter, J. L., "Procedure for Estimating Aerodynamics of Three-Dimensional Bodies in Transitional Flow," *Rarefied Gas Dynamics*, edited by E. P. Muntz, D. P. Weaver, and D. H. Campbell, Vol. 118, Progress in Astronautics and Aeronautics, AIAA, Washington, DC, 1988, pp. 484–492.

[19]Weilmuenster, K. J., Gnoffo, P. A., and Greene, F. A., "Navier-Stokes Simulations of Orbiter Aerodynamic Characteristics with Emphasis on Pitch Trim and Body Flap," AIAA Paper 93-2814, July 1993.

[20]Blanchard, R. C., and Hinson, E. W., "Flight Measurements of Shuttle Orbiter Pitching Moment Coefficient and Elevon Effectiveness in the Rarefied Flow Regime," NASA TP 2889, March 1989.

[21]Koppenwallner, G., and Legge, H., "Drag of Bodies in Rarefied Hypersonic Flow," *Rarefied Gas Dynamics*, edited by J. N. Moss and C. D. Scott, Vol. 103, Progress in Astronautics and Aeronautics, AIAA, Washington, DC, 1985, pp. 44–59.